Steady Shock Refraction in Hypersonic Ramp Flow

Daniel T. Banuti*, Martin Grabe† and Klaus Hannemann‡
German Aerospace Center (DLR), Institute of Aerodynamics and Flow Technology, Göttingen, Germany

This paper discusses features of a supersonic flow with a transversal Mach number stratification when encountering a ramp. A flow of this nature can occur for a variety of reasons around a hypersonic vehicle. Formation of a heated wall boundary layer, external fuel injection on the compression ramp, energy deposition, and film or transpiration cooling are just some of the processes that will establish a flow where a wall near layer features a distinct difference in Mach number compared to the outer flow. This paper will introduce a flow topology framework that will help to understand phenomena associated with this stratification. Shock refraction is identified as the main mechanism which causes a redirection of the flow additional to the ramp deflection. It will be shown how, depending on the Mach number ratios between the layers, shocks or expansion fans will be created that will interact with the surface. This can be the cause for undesired or unexpected temperature and pressure distributions along the wall when shock refraction is not taken into account. As a possible application, it will be shown how shock refraction can act as a virtual external compression ramp. CFD computations are performed using the DLR TAU code, a finite volume, second order accuracy, compressible flow solver.

Nomenclature

M	Mach number	γ	Ratio of specific heats
u	Flow speed	c	Speed of sound
β	Shock angle	ϑ	Deflection angle
$\mathfrak{M}$	Molecular weight	$\mathfrak{R}$	Universal gas constant
p	Pressure	T	Temperature
n	Refractive index	ξ, ζ, η	Fitting parameters
s	Compression stage		

I. Introduction

Significant effort is being made to develop hypersonic vehicles worldwide. The successful American X-43 and X-51 flight experiments show the potential of this approach. European efforts, such as the ATLLAS (see e.g. Longo et al.[7]) and LAPCAT (Steelant[13]) programs focus on civil applications. Sustained hypersonic flight comes with a plethora of problems not encountered in ubiquitous transonic flight. Two main problems are surface heat loads due to high stagnation temperatures and the drag - thrust balance. Many different - and sometimes counterintuitive - steps are being investigated in order to control both problems. Concerning surface heat loads, materials are being developed that can withstand high temperatures (Longo et al.[7]). In this case, the buildup of a high temperature thermal boundary layer along substantial vehicle lengths

*Research Engineer and PhD Student, German Aerospace Center (DLR), Institute of Aerodynamics and Flow Technology, Spacecraft Section, Göttingen, Bunsenstr. 10, Germany, Member AIAA.
†Research Engineer and PhD Student, German Aerospace Center (DLR), Institute of Aerodynamics and Flow Technology, Spacecraft Section, Göttingen, Bunsenstr. 10, Germany.
‡Head of Spacecraft Department, German Aerospace Center (DLR), Institute of Aerodynamics and Flow Technology, Göttingen, Bunsenstr. 10, Germany, Member AIAA.

(e.g. ATLLAS Mach 6 SST: 105 m) is accepted. Other approaches involve active manipulation of the flow. Stalker[12] shows that heat release inside a boundary layer, e.g. due to combustion, can (if done right) reduce surface heat loads, despite the layer of hot gas being introduced in the vicinity of the wall. Schülein[11] shows that energy deposition ahead of a body can be used to reduce both surface heat loads and skin friction, again, despite a region of hot gas being introduced into the incoming flow. Active cooling of the surface using transpiration cooling is part of the SHEFEX II program (Böhrk et al.[4]). Injection of a near wall layer of CO_2 has been shown to delay transition, in turn reducing drag and surface heating (Leyva et al.[6]). Injection of fuel on the compression ramp is an older idea to improve mixing and thus enhance engine efficiency for scramjet engines.

All these approaches have in common that a layer of gas with different properties than the surrounding flow is being introduced into the flow. This might be heated free stream air (energy deposition, thermal boundary layer) or an entirely different gas (ramp H_2 injection, transition delay with CO_2, surface cooling with N_2) or both (intra boundary layer combustion). As vehicle generated shock waves interact with these regions of different speed of sound, the waves will be refracted. This is comparable to the phenomenon of refraction in optics where light is refracted as it passes the interface between two media with a difference in wave propagation speed (e.g. air - water). The phenomenon of shock refraction is being investigated since the late 1940's. Early analytical work has been done by Taub,[14] solving the Rankine-Hugoniot equations assuming a pressure equilibrium and compatible deflection of the waves. He found that shock wave refraction, unlike its optical counterpart, does not allow for total reflection of shocks. Predicted and new wave topologies have been found in experimental work by Abd-El-Fattah and Henderson[1] and have later been duplicated numerically by Colella, Henderson and Puckett.[5]

All these studies have their frame of reference set on either the isolated triple point of incident, transmitted, and refracted wave or regard a moving shock, passing through the interface between two regions of different wave propagation velocity. However, none is concerned with the steady flow around a shock generator itself. Banuti et al.[3] introduced a framework to study these types of flows which are highly relevant for technical applications in super- and hypersonic flight. This paper extends this study and investigates steady shock refraction when stratified flow encounters a ramp and its potential application as a virtual external compression ramp.

II. Methodology

A simplified model setup of stratified flow will be investigated which is based on the Euler equations. A speed of sound stratification of the flow parallel to the adjacent wall and the flow direction will be regarded. Flow velocity and pressure are assumed to be equal in both layers. Wave patterns for the situation when these two layers encounter a ramp will be investigated for both cases of a wall near higher and lower speed of sound compared to the far field. The flow topology will be developed based on physical reasoning, quantitative analysis will be performed using shock-expansion theory. CFD will be used for validation.

II.A. CFD Method

CFD computations are carried out using the DLR TAU Code.[8] TAU is a hybrid grid, Godunov-type finite volume, second order accuracy in space and time, compressible flow solver. It has been verified and is being used for a variety of steady and unsteady flow cases, ranging from sub- to hypersonic Mach numbers, e.g. transonic aerodynamics, atmospheric re-entry, rocket engines, or scramjets. All computations described in this article were based on the Euler equations, using ideal gas thermodynamics for a constant ratio of specific heats $\gamma = 1.4$.

III. Shock Refraction Framework

III.A. Shock Refraction Model

The model is a flow of constant pressure and speed except for a discontinuous stratification parallel to the flow direction. Schematics for the initial flowfield are drawn in Fig. 1. The stratification of speed of sound at constant flow speed causes a stratification in Mach number. The top Mach number region is assumed to extend to infinity. The incoming flow is deflected by an angle ϑ_1 into region 3 upon encountering the ramp. The flow is deflected by this angle all along the oblique shock, forming a virtual ramp for the top

Mach number flow of region 2. However, this initial situation does not remain stable. Being deflected by the

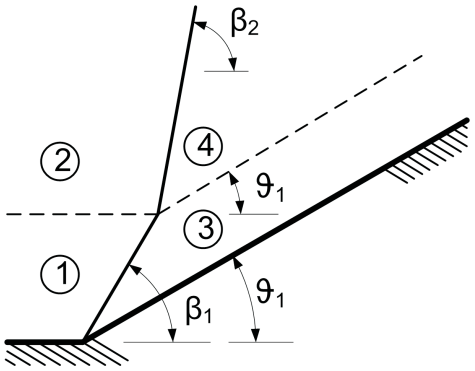

(a) $M_1 > M_2$: Shock refraction type I. Initial shock in region of higher Mach number enters region of lower Mach number.

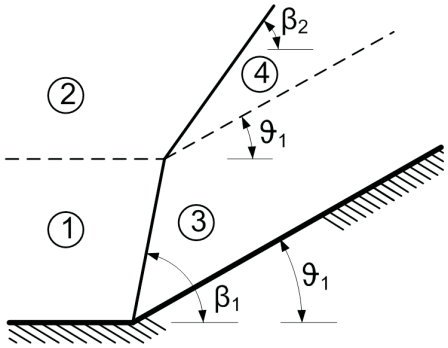

(b) $M_2 > M_1$: Shock refraction type II. Initial shock in region of lower Mach number enters region of higher Mach number.

Figure 1. Shock refraction initial conditions.

same angle, a higher Mach number flow will exhibit a higher post shock pressure. The higher Mach number flow will react to this imbalance by turning into the lower Mach number flow. This will affect the flow fields of Fig. 1 to change to the topologies illustrated in Fig. 2. A shock wave pattern will emerge for $M_2 > M_1$, an expansion wave pattern will form for $M_1 > M_2$. An increase in ϑ_2 will result in an increased pressure in region 5 and a reduced pressure in region 4. Decreasing ϑ_2 has the opposite effect. The deflection additional to the ramp deflection is defined as $\Delta\vartheta = \vartheta_2 - \vartheta_1$. The equilibrium is achieved when equal pressures are reached between regions 5 and 4. The pressure equilibrium mechanism is illustrated in Fig. 3. The plot shows the top layer p_5/p_2 and bottom layer p_4/p_1 pressure ratios for three different Mach numbers each versus the deflection angle $\Delta\vartheta$. The equilibrium condition is $p_5/p_2 = p_4/p_1$. It can be seen how equal top (M_2) and bottom (M_1) Mach numbers yield a zero deflection angle $\Delta\vartheta$. This corresponds to regular homogeneous ramp flow. For $M_1 > M_2$ the equilibrium moves to positive $\Delta\vartheta$, corresponding to type I refraction, Fig. 2(a). $M_1 < M_2$ shifts the equilibrium to negative $\Delta\vartheta$, corresponding to type II refraction, Fig. 2(b). The herein introduced wave topology as well as the pressure equilibrium condition will henceforth be referred to as 'shock refraction framework' (SRF).

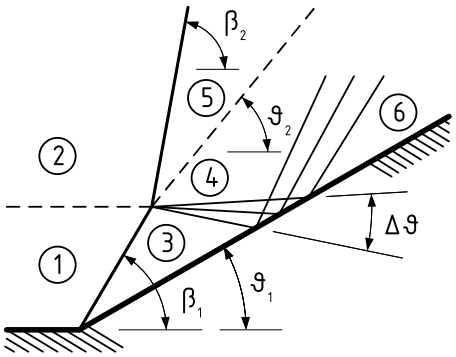

(a) $M_1 > M_2, \Delta\vartheta > 0$: Shock refraction type I. Initial shock reflected as an expansion wave.

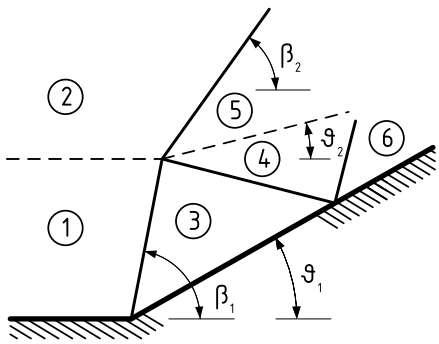

(b) $M_2 > M_1, \Delta\vartheta < 0$. Shock refraction type II: Initial shock reflected as a shock.

Figure 2. Shock refraction equilibrium conditions.

III.B. Validation of Topology

CFD computations of thermally stratified ramp flow have been carried out in order to test this hypothesis. Results can be seen in Fig. 4. Figure 4(a) shows how the oblique shock emanating from the ramp becomes steeper in the high wave speed region while an expansion fan is reflected towards the surface. Case 2 shows a different behavior, as is shown in Fig. 4(b). The shock entering the outer layer is inclined towards the

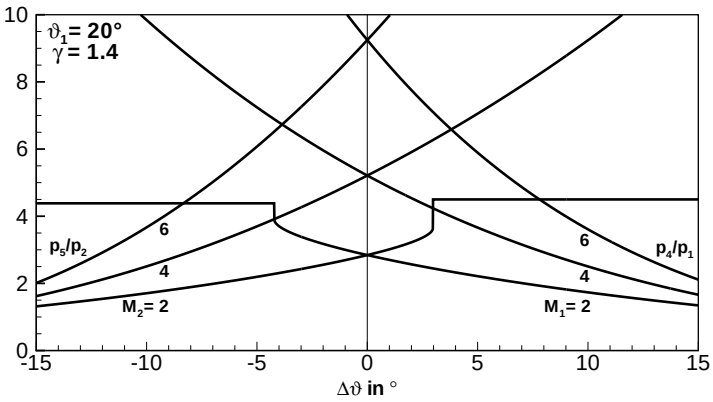

Figure 3. Pressure equilibrium condition.

ramp, a shock is reflected back towards the surface. It can be seen that this shock is repeatedly reflected back and forth between the contact discontinuity and the surface, subsequently decreasing the Mach number and increasing the pressure. It is found that the flow structure simulated using CFD does indeed follow the model.

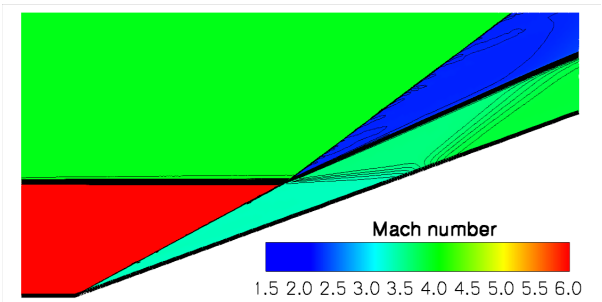

(a) Case 1: High Mach number at bottom (M = 6), low Mach number (M = 4) above.

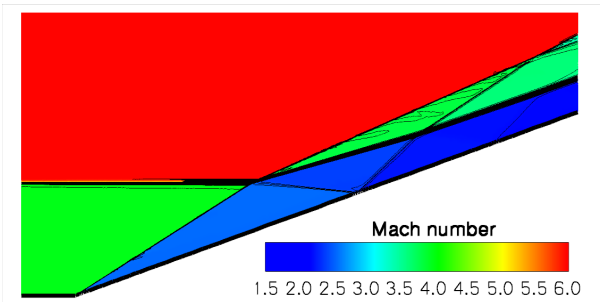

(b) Case 2: Low Mach number (M = 4) at bottom, high Mach number (M = 6) above.

Figure 4. Shock refraction computations at $\vartheta_1 = 20°$ ramp, $\gamma = 1.4$.

III.C. Analysis of the Model

The wave topology and equilibrium condition are identified. The flowfield can now be calculated using Meyer's oblique shock and expansion theory.[9] The equations are translated into a computer program, the solution is thus automated. Free stream Mach numbers M_1 and M_2 as well as the ramp angle ϑ_1 are assumed known. Then, the flow in region 3 is directly given by the oblique shock relations. Region 4 is determined by the deflection $\Delta\vartheta$ from region 3. The equilibrium pressure condition between regions 4 and 5 is used to determine the deflection angle $\Delta\vartheta$. The flow in region 6 can now be calculated by applying an additional deflection by $\Delta\vartheta$ from region 4. This analytical framework has been evaluated numerically to compute exemplary data for the case of a gas of $\gamma = 1.4$ and for several ramp angles.

A map of deflection angle $\Delta\vartheta$ versus the top and bottom Mach numbers is shown in Fig. 5(a) for ramp angles of $\vartheta_1 = 20°$ and $30°$. As expected, the deflection equals zero along the diagonal where $M_1 = M_2$, corresponding to homogeneous ramp flow. The map shows a very regular pattern for slight deviations from the homogeneous case. This highly symmetrical region is bounded to both low M_1 and M_2. This can be understood taking into account Fig. 2. Reducing M_2 with a given M_1 results in a higher deflection angle. The flow in region 2 will eventually not be able to form an attached shock at this ramp and will subsequently detach. This effect can be seen along the near horizontal boundary. Reducing M_1 for a certain M_2 leads to a similar effect. In this case, however, the reflection of the shock wave at the surface will transform to a Mach reflection. If either Mach number passes a lower limiting value, shock separation occurs. Strictly, this condition marks the breakdown of the shock refraction framework as introduced here: regular refraction

requires that incident, transmitted, and reflected shock meet in one triple point. When this is not the case, so-called irregular refration will occur. Comparing Figs. 5(a) and 5(b) shows that larger initial ramp angles require higher Mach numbers for the shocks to stay attached.

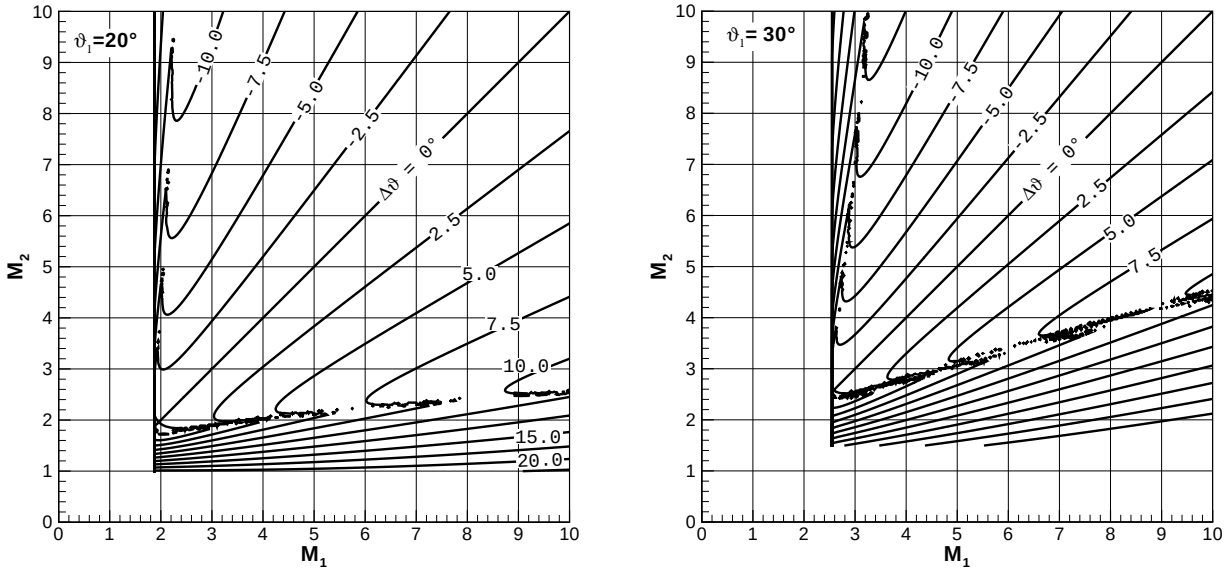

(a) Ramp angle $\vartheta_1 = 20°$

(b) Ramp angle $\vartheta_1 = 30°$

Figure 5. Deflection angle $\Delta\vartheta$ as a function of the free stream Mach numbers from shock refraction framework, $\gamma = 1.4$.

Investigating Fig. 5 more closely, it can be seen that the deflection isocontours in the regular region all intersect in the origin when elongated. This means that, interestingly, for high Mach numbers and moderate angles, the deflection is a function of the Mach number *ratio* and not of the individual Mach numbers. Resulting deflections $\Delta\vartheta$ are read from the plot Fig. 5(a) for the case of $\vartheta_1 = 20°$. Plotting $(\mathrm{M}_2/\mathrm{M}_1)$ as a function of ϑ_2 reveals a hyperbolic nature of this graph. Fitting the data points to a hyperbolic function yields the following parameters:

$$\vartheta_{2,\mathrm{fit}} = \frac{\zeta'}{(\mathrm{M}_2/\mathrm{M}_1) + \xi'}\,; \qquad \zeta' = 41.3248,\ \xi' = 1.06683 \tag{1}$$

Using this formula, the ramp pressure can be directly computed with no need to iteratively determine the equilibrium wave pattern.

III.D. Derivation of a Deflection Equation

It is interesting to see whether the fitted function captures underlying physics. It turns out that an equation of this form can be derived for the case $\mathrm{M}_2 > \mathrm{M}_1$, refer to the schematics shown in Fig. 2(b). In the equilibrium case, equal pressures in regions 5 and 4 have to be established:

$$\frac{p_5}{p_2} = \frac{p_4}{p_1} = \frac{p_3}{p_1}\frac{p_4}{p_3} \tag{2}$$

Using the hypersonic limit of the oblique shock pressure ratio (Anderson[2]) leads to

$$\frac{2\gamma}{\gamma+1}\mathrm{M}_2^2 \sin^2\beta_2 = \frac{2\gamma}{\gamma+1}\mathrm{M}_1^2 \sin^2\beta_1 \cdot \frac{2\gamma}{\gamma+1}\mathrm{M}_3^2 \sin^2\beta_3 \tag{3}$$

Furthermore the hypersonic limit of the post-shock Mach number is used to compute M_3

$$\mathrm{M}_3 = \frac{1}{\sin(\beta_1 - \vartheta_1)}\sqrt{\frac{\gamma-1}{2\gamma}} \tag{4}$$

The shock angles β, with special attention for β_3, are approximated as

$$\beta = \frac{\gamma+1}{2}\vartheta; \qquad \beta_3 = \frac{\gamma+1}{2}(-\Delta\vartheta) \tag{5}$$

Finally assuming small angles, leads, after some algebra, to

$$\vartheta_2 = \frac{\Gamma\vartheta_1}{\mathrm{M}_2/\mathrm{M}_1+\Gamma}\ ; \quad \Gamma = \sqrt{\frac{\gamma+1}{\gamma-1}} \overset{\gamma=1.4}{=} 2.45 \tag{6}$$

Eq. (6) is an improved version of Eq. (1). As a new physical insight, the proportional dependency of ϑ_2 on the initial ramp angle ϑ_1 is revealed. However, Eq. (6) somewhat contradicts Eq. (1), as the analytical model predicts a constant factor Γ, while the fit clearly shows two different values. Combining these two, a new improved fit can be defined which takes into account the ramp angle:

$$\vartheta_2 = \frac{\zeta\vartheta_1}{\mathrm{M}_2/\mathrm{M}_1+\xi}\ ; \qquad \zeta = 2.06624,\ \xi = 1.06683 \tag{7}$$

This new fit Eq. (7) covers a range of ramp angles, as can be seen in Fig. 6.

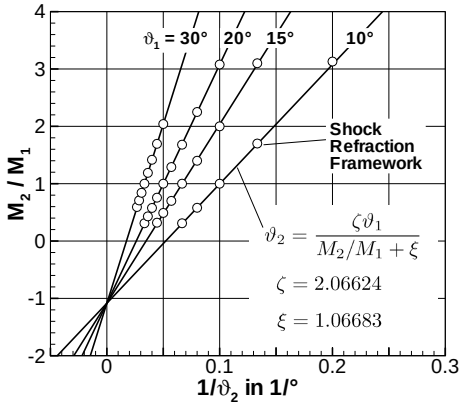

Figure 6. Inverse flow angle ϑ_2 as a function of Mach number ratio $\mathrm{M}_2/\mathrm{M}_1$ for $\gamma = 1.4$. Symbols represent data points read from deflection maps using the shock refraction framework (SRF), lines are drawn using Eq. (7)

III.D.1. Relevance of Mach number ratio

Apparently, the Mach number ratio has been found to be of prime importance in shock refraction. Is there a physical interpretation of this ratio? Keeping in mind that in the beginning, equal flow velocities have been assumed. Then, the Mach number ratio can be transformed as follows:

$$\frac{\mathrm{M}_2}{\mathrm{M}_1} = \frac{u_2/c_2}{u_1/c_1} = \frac{u/c_2}{u/c_1} = \frac{c_1}{c_2} = n \tag{8}$$

The Mach number ratio reduces to the ratio of speed of sound in both layers which is essentially the ratio of wave propagation velocities. Coming full circle to the reference to optical refraction in the beginning of this paper, the ratio of the wave propagation velocities is called refractive index. It is very interesting to see this property, known from a different field of physics, emerge as an important parameter in this fluid dynamic investigation.

III.D.2. Limits of Deflection

Having an equation like Eq. (7) at hand, it can be readily evaluated for limiting cases of M_2/M_1. Interesting cases are $M_2/M_1 \to 0$, $M_2/M_1 \to \infty$, $M_2/M_1 \to 1$.

$$\lim_{M_2/M_1 \to \infty} \left(\frac{\zeta \vartheta_1}{M_2/M_1 + \xi} \right) = \vartheta_2 = 0 \tag{9}$$

$$\lim_{M_2/M_1 \to 1} \left(\frac{\zeta \vartheta_1}{M_2/M_1 + \xi} \right) = \vartheta_2 = \vartheta_1 \tag{10}$$

$$\lim_{M_2/M_1 \to 0} \left(\frac{\zeta \vartheta_1}{M_2/M_1 + \xi} \right) = \vartheta_2 = 2.1\,\vartheta_1 \tag{11}$$

Eq. (9) shows that for $M_2 >> M_1$ the bottom layer is pressed down so much that the upper deflection angle vanishes. $M_2 = M_1$ simply depicts homogeneous ramp flow, hence everything should be deflected by the same angle ϑ_1. Eq. (11) is probably the most interesting case as it has the least obvious result. The incoming flow of region 2 cannot be deflected arbitrarily by increasing M_1. Instead, a maximum upper deflection angle is predicted at approximately twice the physical ramp angle.

III.D.3. One Parameter Equation

The limiting operation of Eq. (10) revealed a connection between the fitting parameters ξ and ζ. Clearly, an appropriate model has to include homogeneous ramp flow. This is the case when Eq. (7) reduces to $\vartheta_2 = \vartheta_1$ for $M_2/M_1 = 1$. This can be used to formulate an additional equation with both fitting parameters:

$$\frac{M_2}{M_1} = 1 \qquad \equiv \qquad \vartheta_2 = \vartheta_1 \qquad \Rightarrow \qquad 1 + \xi = \zeta \tag{12}$$

Using this, the number of fitting parameters can be reduced to unity. The new parameter η is introduced in Eq. (13). It is chosen to underline the difference to ξ, as a new fit with only one degree of freedom has been carried out. Furthermore, Eq. (13) is now expressed solely in terms of the nondimensional ratios ϑ_2/ϑ_1 and M_2/M_1:

$$\frac{\vartheta_2}{\vartheta_1} = \frac{1 + \eta}{M_2/M_1 + \eta}\,; \qquad \eta = 1.06778 \tag{13}$$

Fig. 7 reveals the power of Eq. (13) to reduce data across different ramp angles and Mach number ratios.

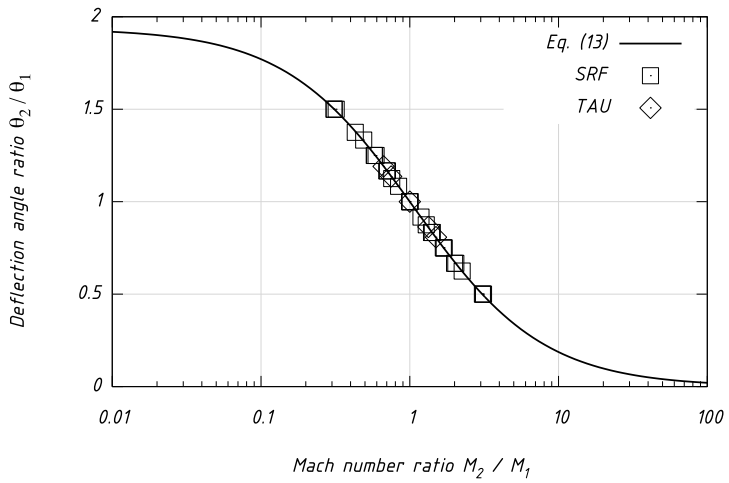

Figure 7. Deflection angle ratio ϑ_2/ϑ_1 as a function of Mach number ratio M_2/M_1. Eq. (13), SRF data of ramp angles $\vartheta_1 = 10°, 15°, 20°, 30°$ and TAU CFD results for $\vartheta_1 = 20°$.

III.E. Influence on Pressure

Now that the deflection angles are known, the shock refraction framework is capable of computing any variable that is predicted by shock-expansion theory. As a first application, a map showing resulting wall pressures as a function of M_1 and M_2 for ramp angles $\vartheta_1 = 20°$ and $30°$ can be seen in Fig. 8. The wall pressures are the pressures in regions 3 and 6, see Fig. 2. Solid lines denote the pressure ratio p_6/p_1 of region 6. The pressure in region 3 is simply the pressure of the regular oblique shock at the ramp and thus not affected by the wave pattern due to refraction. It can be found in the same map along the diagonal, where $M_1 = M_2$.

Along with the pressure ratio the total pressure ratio $p_{0,6}/p_{0,1}$ has been calculated and added to Fig. 8 as dotted lines. For $M_2/M_1 < 1$ (type I, Fig. 2(a)) the vertical distribution and thus independence from M_2 shows that the total pressure loss is determined by the initial oblique shock alone, the isentropic expansion afterwards does not affect the total pressure. For $M_2/M_1 > 1$ (type II, Fig. 2(b)) the losses grow for growing Mach numbers, as the flow passes through two additional shocks to reach region 6. A larger ramp angle result in a higher total pressure loss and increased pressure ratio.

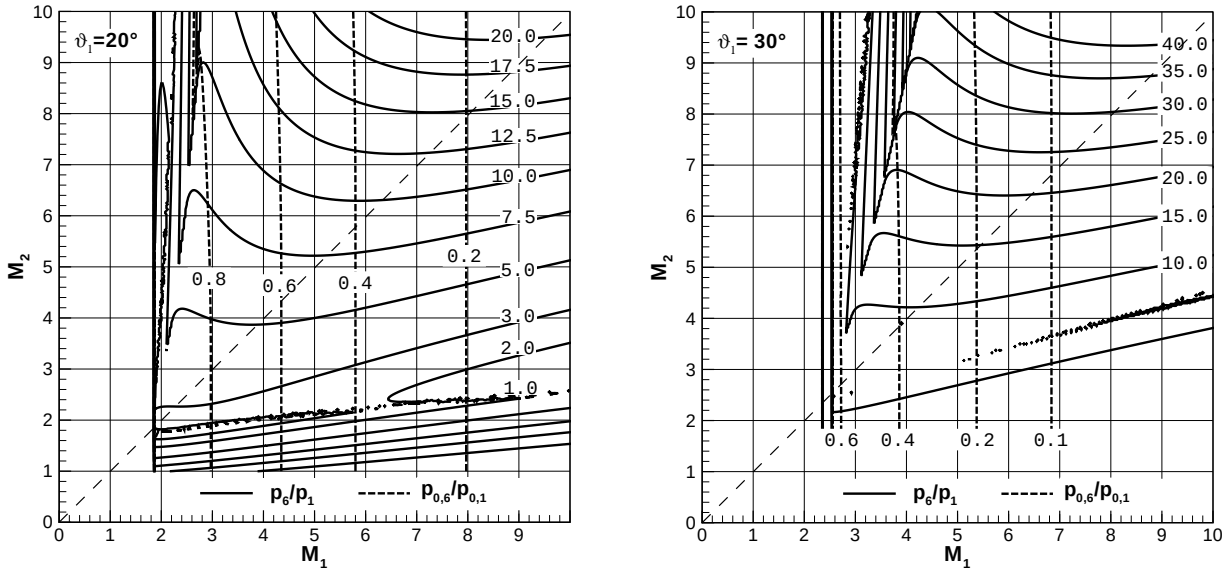

(a) Ramp angle $\vartheta_1 = 20°$.

(b) Ramp angle $\vartheta_1 = 30°$.

Figure 8. Pressure ratio p_6/p_1 and total pressure ratio $p_{0,6}/p_{0,1}$ as a function of the free stream Mach numbers, $\gamma = 1.4$.

III.F. Influence on Temperature

The effect of shock refraction on the temperature is illustrated in Fig. 9, again for ramp angles of $\vartheta_1 = 20°$ and $30°$. Shown is the temperature ratio T_6/T_1, the ratio T_3/T_1 is implicitly included along the diagonal (homogeneous oblique shock from region 1 to 3).

III.G. Comparison with CFD

So far, CFD has only been used qualitatively to assess whether the expected shock patterns can actually occur. As the herein developed shock refraction framework gives detailed numerical data, a quantitative comparison to CFD results can be performed. Table 1 shows total pressure ratio p_{06}/p_{01}, pressure ratio p_6/p_1, temperature ratio T_6/T_1 and deflection angle ratio ϑ_2/ϑ_1 as obtained by the TAU code and the shock refraction framework. The angle ratio ϑ_2/ϑ_1 from Eq. (13) is also added. The relative error compared to TAU CFD results is given. Excellent agreement has been found between CFD, SRF and Eq. (13).

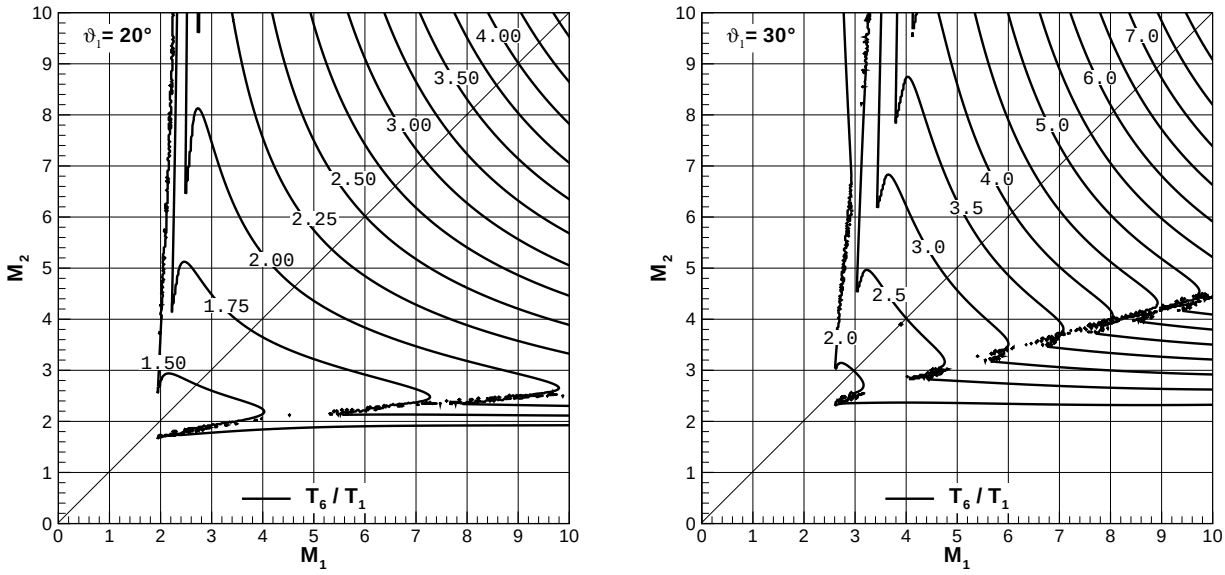

(a) Ramp angle $\vartheta_1 = 20°$.

(b) Ramp angle $\vartheta_1 = 30°$.

Figure 9. Temperature ratio T_6/T_1 as a function of the free stream Mach numbers, $\gamma = 1.4$. T_3/T_1 is included implicitly along the diagonal.

Case						
	M_1	4.0000E+0	6.0000E+0	6.0000E+0	8.0000E+0	6.0000E+0
	M_2	6.0000E+0	8.0000E+0	6.0000E+0	6.0000E+0	4.0000E+0
	M_2/M_1	1.5000E+0	1.3333E+0	1.0000E+0	7.5000E-1	6.6667E-1
CFD TAU	p_{06}/p_{01}	6.4848E-1	3.7477E-1	3.7712E-1	1.9708E-1	3.7591E-1
	p_6/p_1	8.5692E+0	1.4506E+1	9.2464E+0	8.4592E+0	4.6008E+0
	T_6/T_1	2.0894E+0	2.8423E+0	2.4946E+0	2.9275E+0	2.0455E+0
	ϑ_2/ϑ_1	8.0759E-1	8.6372E-1	1.0000E+0	1.1364E+0	1.1908E+0
SRF	p_{06}/p_{01}	6.5034E-1	3.7548E-1	3.7636E-1	1.9796E-1	3.7636E-1
	p_6/p_1	8.5807E+0	1.4521E+1	9.2458E+0	8.4668E+0	4.5855E+0
	T_6/T_1	2.0898E+0	2.8415E+0	2.4960E+0	2.9244E+0	2.0428E+0
	ϑ_2/ϑ_1	8.0712E-1	8.6373E-1	1.0000E+0	1.1357E+0	1.1903E+0
Eq. (13)	ϑ_2/ϑ_1	8.0530E-1	8.6119E-1	1.0000E+0	1.1375E+0	1.1922E+0
Error SRF	p_{06}/p_{01}	2.8586E-3	1.8914E-3	-2.0096E-3	4.4623E-3	1.1929E-3
	p_6/p_1	1.3367E-3	1.0123E-3	-6.2731E-5	8.8700E-4	-3.3235E-3
	T_6/T_1	1.9554E-4	-2.7870E-4	5.3217E-4	-1.0367E-3	-1.3187E-3
	ϑ_2/ϑ_1	-5.7302E-4	1.8524E-5	0.0000E+0	-6.2824E-4	-4.4484E-4
Error Eq. (13)	ϑ_2/ϑ_1	-2.8425E-3	-2.9341E-3	0.0000E+0	9.5713E-4	1.1029E-3

Table 1. Comparison of CFD, shock refraction framework (SRF) and analytical result for $20°$ ramp angle, $\gamma = 1.4$. Error is relative error compared to TAU results.

IV. Practical Considerations

IV.A. Manipulating the Local Mach Number

In order to use shock refraction in a technical application, the stratification itself and a technical realization should be addressed. First of all, how can a local wave velocity be manipulated? For an ideal gas,

$$c = \sqrt{\gamma \frac{\mathfrak{R}}{\mathfrak{M}} T} \tag{14}$$

where $c, \gamma, \mathfrak{R}, \mathfrak{M}, T$ are speed of sound, ratio of specific heats, universal gas constant, molecular weight, and temperature, respectively. Equation (14) shows that a local speed of sound can be affected by changing the composition of the gas (γ and $\mathfrak{M}$) and its temperature T. The speed of sound can thus be reduced, in turn increasing the Mach number, by

- increasing molecular weight $\mathfrak{M}$, e.g by replacing air with CO_2
- reducing the ratio of specific heats γ, e.g. by introducing a gas with less degrees of freedom
- reducing gas temperature T, e.g. by surface cooling, injecting cooled air, or vaporization of liquid sprays

The speed of sound can be increased, in turn reducing the Mach number, by

- decreasing $\mathfrak{M}$, e.g. by replacing air with H_2 or He
- increasing γ, e.g. by introducing a gas with more degrees of freedom
- increasing T, e.g. by surface heating, energy deposition, combustion, injecting hot exhaust gases

It appears practical that one layer would be modified while the second layer remains at free stream conditions. Then, four different cases can be distinguished[a].

IV.A.1. M_2 *is free stream,* M_1 *is increased*

In this case, an expansion wave pattern will occur, as depicted in Fig. 2(a). Film cooling and CO_2 transition damping may cause this. Fig. 8 shows the resulting minor reduction in static pressure at the surface at substantially increased total pressure loss. Fig. 9 reveals the increase in temperature compared to the homogeneous flow case. This effect might partially reduce the effectiveness of film cooling.

IV.A.2. M_2 *is free stream,* M_1 *is decreased*

Fig. 2(b) shows the resulting shock pattern of this case. It may occur when a thermal boundary layer develops to significant dimensions along the hot wall of a hypersonic vehicle. Another likely option is wall near hydrogen fuel injection. The static pressure (Fig. 8) is found to change only mildly whereas the total pressure loss may reduce significantly. Fig. 9 furthermore shows the reduction in temperature gain. With these characteristics, this condition may be well suited as an engine inlet, technical realization seems feasible.

IV.A.3. M_1 *is free stream,* M_2 *is increased*

A shock pattern will establish, see Fig. 2(b). Manipulation of region 2 requires a mechanism that is active over a certain distance or the manipulation needs to be brought into the flow upstream. This appears to be the technically most challenging case, as remote cooling or introduction of a gas is not straightforward. Liquid spray injection, say for a hydrocarbon fuel, seems to be a promising candidate. In this way, vaporization will decrease the gas temperature. Fig. 8 reveals how the pressure ratio can be increased at an essentially constant total pressure loss with this configuration. Furthermore, it can be seen along the diagonal which higher free stream Mach number in a homogeneous flow is needed to create this pressure - with associated higher total pressure loss. Fig. 9 shows how the associated temperatures can be reduced.

[a]The reasoning can best be followed by starting at a point, say $M_1 = M_2 = 6$, which represents the free stream condition and regular wedge flow of a homogeneous medium. Then, follow in the direction of the manipulated stream, e.g. upwards when M_2 is increased, to the left when M_1 is decreased, and so on.

IV.A.4. M_1 *is free stream,* M_2 *is decreased*

Fig. 2(a) shows the expansion wave pattern of this case. It can occur for off wall energy deposition, or upstream off wall injection of hydrogen fuel. As Figs. 8 and 9 show, this will reduce the static pressure and the temperature at the wall. This might hence be a way to reduce thermal and mechanical loads to surfaces or to reduce drag.

IV.B. Compression Ramp

As one possible application, a shock refraction enhanced compression ramp is discussed. Typically, using a compression ramp as an engine inlet, the design goal is to create high pressures with minimal losses. Both factors can be addressed using shock refraction for a given ramp. Due to the nonlinear relation between shock strength and total pressure loss, theoretically a compression using as many compression steps as possible is optimal, as it minimizes the losses. Technically, two or three steps are typically used.[10] Using a one step compression is clearly undesirable from this point of view. However, a type II shock refraction may serve as an external virtual compression ramp which will introduce several compression steps, Fig. 10(a). The subsequent additional deflection induced by the pressure equilibrium mechanism is equivalent to an external ramp, Fig. 10(b).

Figure 8 shows how pressure and total pressure loss are affected. As an illustrative example, a vehicle

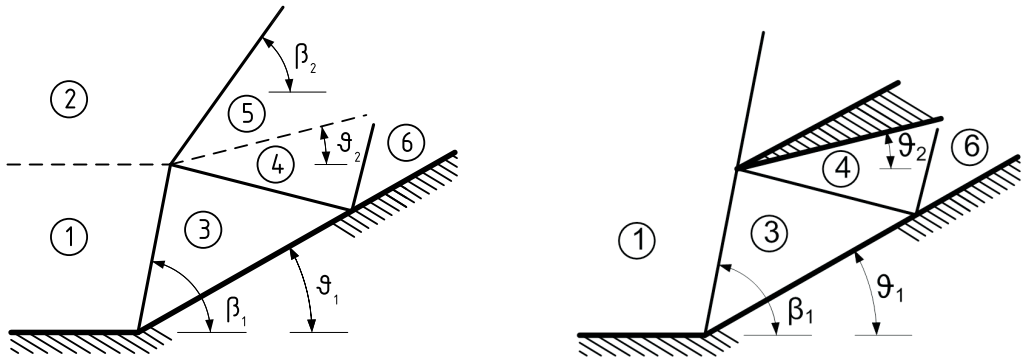

(a) $M_2 > M_1$: Shock refraction type II. (b) Equivalent external compression ramp.

Figure 10. Virtual external compression ramp.

flight Mach number of six is chosen. The undisturbed ramp without refraction exhibits a pressure ratio of $p_6/p_1 = 9.25$ and a total pressure ratio of $p_{0,6}/p_{0,1} = 0.3764$. In order to increase the compression, the off wall Mach number M_2 has to be increased. Choosing e.g. $M_2 = 8$ yields a pressure ratio of $p_6/p_1 = 14.52$ and a total pressure ratio of $p_{0,6}/p_{0,1} = 0.3755$. This means that the pressure could be increased by more than 50% while the increase in total pressure loss is negligible. Keeping $M_2 = 6$ and decreasing M_1 to 5 instead mainly effects the total pressure loss: this approach yields a pressure ratio of $p_6/p_1 = 9.18$ and a total pressure ratio of $p_{0,6}/p_{0,1} = 0.5048$. Figure 8 shows that this effect gets stronger for higher baseline Mach numbers.

Is it possible to adjust the refraction to fulfill Oswatitsch's condition of equal shock strengths? Oswatitsch[10] restates this condition as $M_s \sin\beta_i = \text{const}$ where s is the index of subsequent compression stages. This can again be rewritten using the hypersonic limits for β and assuming small angles.

$$M_s \sin\beta_s = \text{const} \rightarrow M_s \frac{\gamma+1}{2}\vartheta_s = \text{const} \tag{15}$$

As the Mach number decreases across a shock, the deflection angle needs at least to stay constant. As limiting case, it will be investigated if the subsequent deflection angle $-\Delta\vartheta$ can reach the value of the ramp angle ϑ_1[b]. Equation 7 has been derived to facilitate a simple estimation of the subsequent deflection angle. With (per definition) $\vartheta_2 = \vartheta_1 + \Delta\vartheta$ and $-\Delta\vartheta = \vartheta_1$ however, Eq. (7) only yields $0 = 0$. What happened? The answer can be seen in Fig. 10(a). In order to have equal deflection angles, $\Delta\vartheta = -\vartheta_1$. Hence, $\vartheta_2 = \vartheta_1 + \Delta\vartheta = 0$, i.e.

[b]Here, an alternative line of argument is given compared to the limiting investigation performed earlier.

the virtual ramp angle has to vanish. However, in this case no deflection in region 2 takes place, no shock is formed and the pressure equilibrium between regions 5 and 4 is turned impossible. It could thus be shown that Oswatitsch's ideal, equal deflection angles compression cannot be realized using a shock refraction ramp.

V. Compression Cascade

So far, analysis has been limited to the reflection of the refracted wave at the surface, dubbed region 6 (compare Fig. 1). However, as can already be expected from this schematic drawing, further interaction of the waves with each other and the contact discontinuity is very likely. In fact, the CFD result in Fig. 4(b) shows a faint shock being reflected back from the interface and then again reflected from the wall, resulting in a rather complicated shock wave pattern. Is it possible to analyse this topology further?

V.A. Simplified Cascading Model

It turns out that this is indeed the case if an additional constraint is introduced: the transmitted shocks passing from the lower layer into the upper layer are assumed to not interact with each other, so that shocks that are formed in this interaction are not being reflected back to the ramp. This is depicted in Fig. 11(a).[c]
It can then be seen in Fig. 11(a) that the initial λ-like wave pattern around the triple point of of impinging,

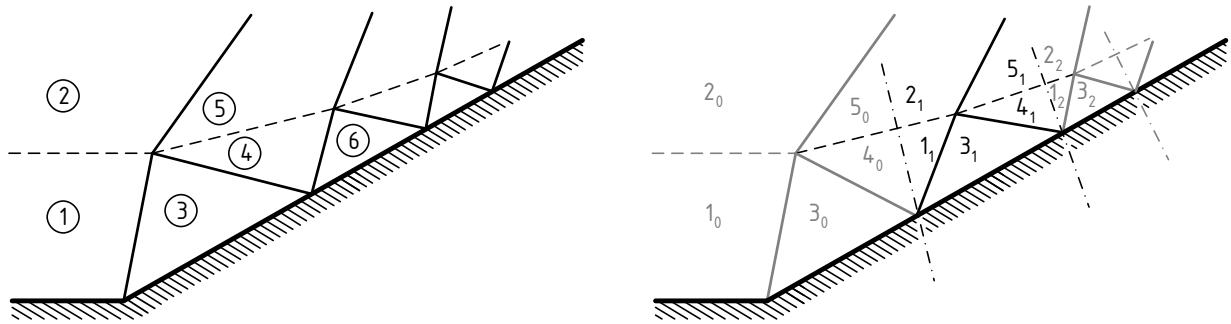

(a) Schematic of independent cascade shock topology. (b) Compression stage concept of independent cascade model.

Figure 11. Cascaded independent compression stages model.

transmitted, and refracted shock is seen to repeat afterwards, becoming smaller and smaller. Each pattern can be understood as a new refraction problem: the flow in regions 5 and 4 is deflected by an angle $\Delta\vartheta$ towards the ramp wall while different Mach numbers prevail in each region. Thus, again, a stratified flow is facing being deflected by a wall.

V.B. Numerical Evaluation of the Cascade Model

Fig. 11(b) illustrates how the flow in regions 4 and 5, after the first compression stage, can be understood as the initial flow for a second stage and so on. Region 6 can thus be reinterpreted as a region 3 of a second compression stage. It is then possible to numerically evaluate the cascading flow pattern using the SRF by calling a new refraction problem, using the conditions in 5 and 4 as initial conditions 2 and 1 of the subsequent problem. An exemplary result of a cascade at a 20° ramp with $M_1 = 4$ and $M_2 = 6$ can be seen in Fig. 12. Plotted is the evolution of Mach numbers and the ratio of local pressure to the initial pressure. Index s denotes the number of the stage.

It can be seen that, while the cascades theoretically repeat ad infinitum, a limiting value is reached after a few stages for pressures and Mach numbers. After stage 4, conditions do not change significantly. The difference in Mach number is found to prevail, the pressure is seen to converge towards a common limiting value. The flow direction $\vartheta_{2,s}$ asymptotically approaches the ramp angle. With vanishing difference in pressure, the local deflection angle $\Delta\vartheta_s$ vanishes as well. It can be seen that the bottom gas layer is being significantly compressed beyond the regular oblique shock compression at the ramp.

[c]In fact, this constraint does not seem too limiting: for lower Mach numbers, the upward shocks run at steep angles and will thus meet far away. For higher Mach numbers, the shocks run almost horizontally, thus any interaction will be felt far downstream.

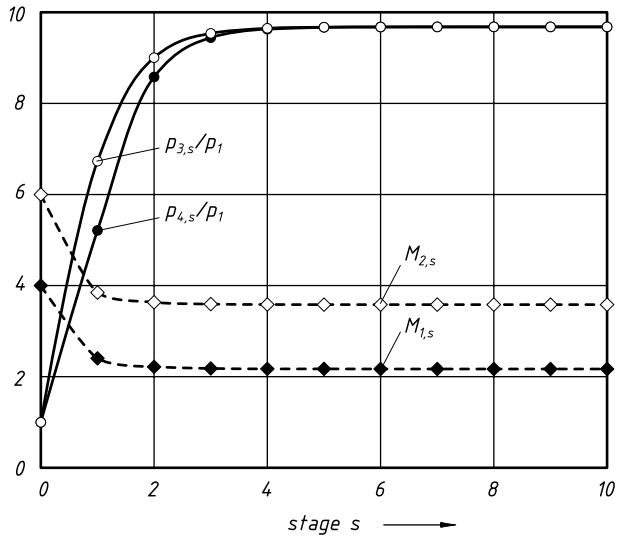

Figure 12. Compression cascade. Plotted is the change in Mach number and pressure ratio. Lines are drawn merely to illustrate the trend, as discrete stages are being evaluated.

VI. Summary and Conclusion

The occurrence of stratified flow in recent hypersonic technology investigations is apparent. Relevant processes are formation of a heated wall boundary layer, external fuel injection on the compression ramp, energy deposition, film or transpiration cooling. When flow of this kind encounters a compression ramp, a shock refraction wave pattern will establish. Shock refraction will change wall surface pressure and temperature distributions as well as create shock or expansion waves that may interact with the wall in unexpected ways.

A framework has been developed, based on a shock refraction mechanism, that formalizes the wave topology. A deflection additional to the initial ramp deflection has been identified as a prime characteristic, determined by a pressure equilibrium condition. Based on the shock refraction framework, shock expansion theory has been used to to compute pressures and temperatures in the flow field. Comparison with CFD results obtained with the DLR TAU code shows excellent agreement.

It could be shown that in the majority of cases where regular refraction occurs, deflection is a function of the Mach number ratio alone, instead of actual individual Mach numbers. An equation could be derived based on hypersonic flow theory that exhibits the characteristics of the previously found dependence. Ultimately, we succeeded in reducing data over wide ranges of Mach numbers and ramp angles into a single equation. Again, agreement with CFD is excellent. The Mach number ratio as dominant parameter of the flow has been shown to be linked to the refractive index known from optics. It is noteworthy that the found equation covers the whole Mach number ratio domain despite having been derived for the case of a shock only pattern (i.e. $M_2 > M_1$).

Technical realization and implications have been discussed, most notably drag reduction and engine inlet improvement. It has been shown that a reduction in film cooling efficiency might occur due to shock refraction.

Finally, a generalization of the initial wave pattern to a compression cascade has been carried out. It could be shown that the additional deflection $\Delta\vartheta$ will vanish, as pressures equilibrate. The final pressure reached might be significantly higher than the pressure reached in the initial stage.

Acknowledgments

This work has in part been carried out within project ATLLAS (Aerodynamic and Thermal Load Interactions with Lightweight Advanced Materials for High Speed Flight) which is coordinated by ESA-ESTEC and supported by the EU within the 6th Framework Program, Aeronautic and Space, Contract no.: AST5-CT-2006-030729.

References

[1]A.M. Abd-El-Fattah and L.F. Henderson. Shock waves at a fast-slow gas interface. *Journal of Fluid Mechanics*, 86(1):15–32, 1978.

[2]J.D. Anderson. *Hypersonic and High-Temperature Gas Dynamics*. AIAA, 2nd edition, 2006.

[3]D.T. Banuti and K. Hannemann. Flow control by energy deposition in hypersonic flow - some fundamental considerations. In *Proceedings of the 16th AIAA/DLR/DGLR International Space Planes and Hypersonic Systems and Technologies Conference*, number AIAA-2009-7345, Bremen, Germany, 2009. AIAA/DLR/DGLR.

[4]H. Böhrk, O. Piol, and M. Kuhn. Heat balance of a transpiration-cooled heat shield. *Journal of Thermophysics and Heat Transfer*, 24(3):581–588, 2010.

[5]P. Colella, L.F. Henderson, and E.G. Puckett. A numerical study of shock wave refractions at a gas interface. In *Proceedings of the 9th AIAA Computational Fluid Dynamics Conference*, Buffalo, USA, 1989. AIAA.

[6]I.A. Leyva, S. Laurence, A.W.-K. Beierholm, H.G. Hornung, R. Wagnild, and G. Candler. Transition delay in hypervelocity boundary layers by means of CO2/acoustic instability reactions. In *Proceedings of the 47th AIAA Aerospace Sciences Meeting Including The New Horizons Forum and Aerospace Exposition*, Orlando, USA, 2009. AIAA.

[7]J.M.A. Longo, R. Dittrich, D. Banuti, M. Sippel, J. Klevanski, U. Atanassov, G. Carrier, Ph. Duveau, I. Salah El Din, R. Thepot, A. Loubeau, F. Coulouvrat, R. Jarlas, H. Rabia, D. Perigo, and J. Steelant. Concept study for a mach 6 transport aircraft. In *Proceedings of the 47th AIAA Aerospace Sciences Meeting*, number AIAA-2009-435, Orlando, USA, 2009.

[8]A. Mack and V. Hannemann. Validation of the unstructured DLR-TAU-code for hypersonic flows. In *Proceedings of the 32nd AIAA Fluid Dynamics Conference and Exhibit*, number AIAA-2002-3111, 2002.

[9]T. Meyer. *Über zweidimensionale Bewegungsvorgänge in einem Gas, das mit Überschallgeschwindigkeit strömt.* PhD thesis, Georg August Universität Göttingen, 1908.

[10]K. Oswatitsch. *Gasdynamik*. Springer, 1952.

[11]E. Schülein and A. Zheltovodov. Effects of localized flow heating by dc-arc discharge ahead of non-slender bodies. In *Proceedings of the 16th AIAA/DLR/DGLR International Space Planes and Hypersonic Systems and Technologies Conference*, Bremen, Germany, 2009. AIAA/DLR/DGLR.

[12]R.J. Stalker. Control of hypersonic turbulent skin friction by boundary-layer combustion of hydrogen. *Journal of Spacecraft and Rockets*, 42(4):577–587, 2005.

[13]J. Steelant. Achievements obtained for sustained hypersonic flight within the LAPCAT project. In *Proceedings of the 15th AIAA International Space Planes and Hypersonic Systems and Technologies Conference,*, number AIAA-2008-2578, Dayton, USA, 2008.

[14]A.H. Taub. Refraction of plane shock waves. *Physical Review*, 72(1):51–60, 1947.